Multifunctional Single Layer Metasurface Based on Hexagonal Split Ring Resonator

MUHAMMAD SALMAN WAHIDI[1], **M. ISMAIL KHAN**[2,3],
FAROOQ A. TAHIR[1]**, (Senior Member, IEEE), AND HATEM RMILI**[4]**, (Senior Member, IEEE)**
[1]Research Institute for Microwave and Millimeter-Wave Studies, National University of Sciences and Technology (NUST), Islamabad 44000, Pakistan
[2]School of Optics and Photonics, Beijing Institute of Technology, Beijing 100081, China
[3]Department of Electrical Engineering, COMSATS University, Attock Campus, Islamabad 44000, Pakistan
[4]Electrical and Computer Engineering Department, Faculty of Engineering, King Abdulaziz University, Jeddah 21589, Saudi Arabia

Corresponding author: Farooq A. Tahir (farooq.tahir@seecs.edu.pk)

ABSTRACT We present a single-layer metasurface, which performs both cross and circular polarization conversion at multiple frequency bands. The unit cell of the proposed metasurface consists of periodic array of a uniquely designed hexagonal split ring resonator (SRR). The proposed metasurface behaves as an efficient 90° polarization rotator at dual frequency bands of 6.36-6.59 GHz and 10.54-13.56 GHz. The polarization conversion efficiency approaches 90% within these two operating bands. Moreover, linear-to-circular polarization conversion is also achieved in other three wide frequency bands from 6.10-6.20 GHz, 6.84-9.02 GHz and 14.10-15.48 GHz. The novel features of the subject hexagonal metasurface, which qualify it for numerous practical applications are high cross-polarization conversion (CPC) efficiency, wideband operation and angular stability for oblique incidence up to 45°.

INDEX TERMS Metasurface, angular stability, polarization conversion, PCR, CP, CPC.

I. INTRODUCTION

Metasurfaces offer unprecedented opportunities to control and manipulate the amplitude, phase and polarization of electromagnetic waves. Since, the sub wavelength unit cell of the metasurface can be engineered to achieve any desirable functionality; therefore, they have found potential use in many applications such as antenna gain enhancement [1], radar cross section reduction [2], flat lensing [3], beam splitting [4], real-time holograms [5], absorbers [6]–[8], metasurface antennas [9], [10], polarization conversion and chipless radio-frequency identification (RFID) tags [5], [11]–[13]. Owing to its key role in many applications, the polarization control of EM waves has always been of central interest to scientific and engineering community. Although, polarization can be manipulated through conventional techniques, such as by passing a wave through an anisotropic material where phase difference is accumulated as the wave propagates through the material, however, these techniques have

narrow bandwidth and require bulky size when the operating wavelength is large.

In order to achieve polarization control through compact structures, researchers have shifted their focus towards meatasurfaces. In this regard, broadband linear polarization rotators have been reported in the recent literature at microwave frequencies [12]–[16]. Highly efficient transparent 90° polarization rotator is achieved based on U-shaped periodic array using combined chirality and tunneling that operates over frequency range of 9.8-12.5 GHz [17]. A cross polarizer is exhibited making use of multi-order plasmon resonances and high impedance surfaces [18], however these designs only work for narrow bandwidth. Ultra-wideband (7.57-20.46 GHz) cross-polarization conversion (CPC) has been demonstrated through an anisotropic metasurface consisting of square-shaped resonators [19]. However, this polarizer only works for normal incidence. The existing literature indicates that metasurfaces have also been realized with good angular stability [20], [21]. A dual-broadband two-slit rectangular split-ring resonator anisotropic metasurface [22] achieves angular stability up to 60°, however, the polarization conversion efficiency is quite low that is up to 60%.

Highly efficient polarization rotators have also been presented recently with polarization conversion ratio (PCR) above 90% [23]–[25] but these metasurfaces have obvious disadvantage of not being angular stable.

Linear-to-circular or circular-to-linear polarization converting metasurfaces have also been proposed for operation in microwave frequency regime [26]–[35], however most of them either do not possess angular stability or they have multilayer structures and hence not easily fabricable. The designs discussed so far, though, realize polarization control through planar metasurfaces, however, either they have only one type of polarization control either linear or circular, or have severe shortcomings regarding angular stability, operating bandwidth, and efficiency. For many practical applications, multifunctional metasurfaces with both angularly stable linear and circular polarization control capabilities are of great potential [36]–[42]. Mao *et al.* proposed a broadband multifunctional reflective metasurface for both linear and circular polarization conversion operations with angular stability up to 30° [36].

The major drawback of this design is its reduced bandwidth for HWP and QWP operations at higher oblique incidence angles. A bi-layer anisotropic metasurface has been designed working in transmission mode [43]. However, the proposed design gives very narrowband operation only at resonance frequencies of 16.7 GHz and 19.25 GHz. Some designs with narrowband operations both in transmission and reflection modes have also been reported [44]–[50].

The summary of the above literature review is that designing an angularly stable multifunctional metasurface with high polarization conversion efficiency and wide bandwidth on a single layer substrate is a challenging task. As it can be observed in the comparison table of metasurface, all previously published metasurfaces have employed either circular, square, rectangular or other arbitrary shapes. In this proposed design, hexagonal ring is utilized. It has obvious advantages such as, higher packing efficiency, large electrical length in small area, thus lower operating frequency and in return, higher fractional bandwidth, and greater angular stability due to smaller periodicity. In this research, the authors have tried to meet this challenge, and have successfully demonstrated a multifunctional multi-broadband angularly stable single layer metasurface through a novel hexagonal meta-atom.

TABLE 1. Comparison of metasurfaces.

Research paper	Unit-cell	Operation (cross- and circular polarizer)	Frequency range (in GHz), Efficiency, Angular Stability
Journal of Applied Physics 117.4 (2015): 044501	Diagonal metallic strip	Circular	11-18.3, 80%, 40⁰
Progress In Electromagnetics Research 155 (2016): 115-125	Cross sign	Circular and Gain Enhancement	9.12-10.2, NA, NA
Radio Science, Vol. 52, pp. 1395-1404, 2017	Circular Split-Ring	Cross	6.06-15.98, ~80%, 45⁰
Journal of Physics D: Applied Physics 50.43 (2017): 43LT04	Slotted-square	Cross & circular	16.7 (Cross), 19.25 (Circular), 90%, ~30⁰ (for Circular)
Applied Physics A 123, 767, doi: 10.1007/s00339-017-1322-6 (2017)	Double L-shaped	Cross & circular	5.5-22.75 (three resonances for Cross & four non-resonance bands for Circular), ~90%,30⁰
IEEE Transactions on Antennas and Propagation 66.6 (2018): 3213-3218	Patch array	Cross	8.5-11.56, ~99%, 0⁰ (normal incidence)
Japanese Journal of Applied Physics 57.9 (2018): 090311	Multi V-Shaped	Cross	14.2-43.2, ~96%, 0⁰ (normal incidence)
Optics express 26.20 (2018): 26235-26241	Double slotted squares	Cross	16.67-17.1, ~90%,NA
Scientific reports 8.1 (2018): 1051	Double fishbone structure	QWP	7-9.2, NA, 10⁰
IEEE International Symposium on Antennas and Propagation, pp. 777-778, 8-13(2018)	Two quarter rings	Cross & circular	Cross (resonances at 9.20, 17.85, 20.37) & circular (9.97-15.93), ~99%
Physical Review Applied 11.4 (2019): 044042	Rectangle shaped	QWP	6.73-7.60, NA,NA
Sci Rep 9, 4552 (2019)	Fish structure	Cross & circular	Cross (8-11) & circular (7.5-7.7 & 11.5-11.9), 95%, 45⁰

II. METASURFACE DESIGN

A. GEOMETRICAL CONFIGURATION

The proposed metasurface, shown in Fig. 1, consists of two-dimensional periodic arrangement of unit cells along *x*- and *y*- axes. The unit cell is composed of a metallic hexagonal split ring placed on the top of FR4 dielectric substrate with metallic ground plane. The FR4 is an inexpensive substrate that has relative permittivity of 4.3 and loss tangent of 0.025. The Hexagonal split ring and ground plane are made of copper with conductivity of 5.8×10^7 S/m having thickness of $17 \mu m$.

The optimized dimensions of the structure are given in millimeters: d= 0.6, $L_1 = 2.60$, $L_2 = 3$, $L_3 = 1$, $L_4 = 2.88$, $L_5 = 2.30$, $L_6 = 2.30$, $L_7 = 0.85$, $L_8 = 1.96$, w= 1, the thickness *t* of the substrate is 2.4mm with periodicity of the unit cells p= 8mm.

III. PERFORMANCE ANALYSIS

A. CROSS POLARIZATION CONVERSION

The proposed metasurface behaves as an efficient and broadband 90° polarization plane rotator. The surface is optimized
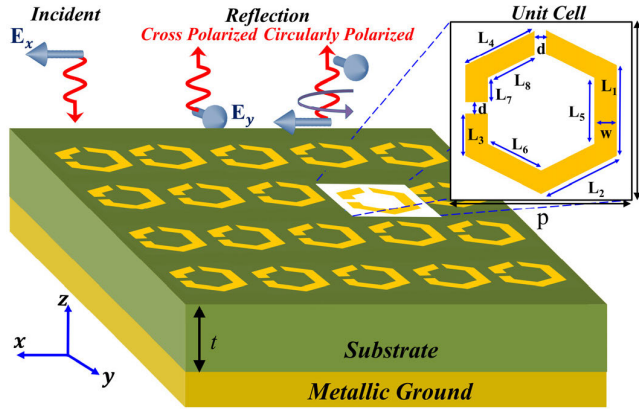
FIGURE 1. Schematic diagram of designed hexagonal metasurface. Inset shows the front view of unit cell. The yellow part is made of copper.

(a)

(b)

FIGURE 2. Magnitude of co- and cross-polarized reflection coefficients for (a) *y*-polarization (b) *x* -polarization.

through extensive parametric analysis giving a broadband response as shown in Fig. 2. It is pertinent to mention here that as a general criterion for cross-polarization conversion (CPC), the magnitude of co-polarized reflection coefficients should be less than -3 dB ($R_{xx} < -3\ dB$ and $R_{yy} < -3\ dB$) or equivalently cross-polarized reflection coefficients should be greater than -3 dB ($R_{yx} \geq -3\ dB$ and $R_{xy} \geq -3\ dB$), for this criterion, cross-polarization efficiency remains 70%. However, a cross polarizer is considered highly efficient if the magnitude of co-polarized reflection coefficients is less than -10 dB ($R_{xx} < -10\ dB$ and $R_{yy} < -10\ dB$) or equivalently cross-polarized reflection coefficients is greater than -2 dB ($R_{yx} \geq -2\ dB$ and $R_{xy} \geq -2\ dB$), for this second criterion, cross-polarization efficiency reaches 90%. In this perspective, if we look at CPC results shown in Fig. 2 (a)-(b), the magnitude of co-polarized reflection coefficients for both x and $y-$ polarized incident waves are below -10 dB within the two operating bands. CPC operation is achieved from 6.36-6.59 GHz and 10.54-13.56 GHz, where x-polarization is converted into y-polarization and vice-versa. Moreover, the cross-polarized reflection coefficients are maximum at three resonance frequencies where the first resonance occurs at 6.6 GHz while the second and third resonances are occurring at 11 GHz and 12.5 GHz. The two nearby resonances occurring at 11 GHz and 12.5 GHz help in extending the bandwidth of the second band (10.54-13.56 GHz).

B. CIRCULAR POLARIZATION CONVERSION
Another very important function that the proposed metasurface performs is linear to circular polarization conversion. The ideal conditions required for this operation (linear to circular polarization conversion and vice versa) are that the amplitude of the orthogonal electric field components (co- and cross-polarized) must be same $\left(|R_{xy}| - |R_{yy}| = 0\ \text{dB}\right)$ while their phase difference must be odd multiple of 90°

$$\left(\Delta\emptyset = \emptyset_{xy} - \emptyset_{yy} = n^{\pi}/_2\right) \quad (1)$$

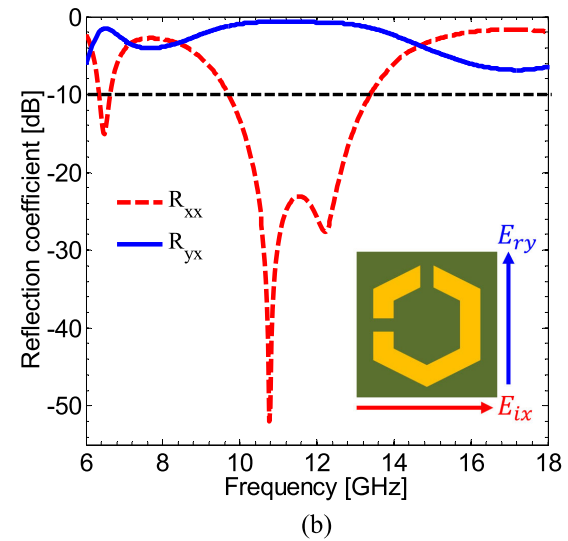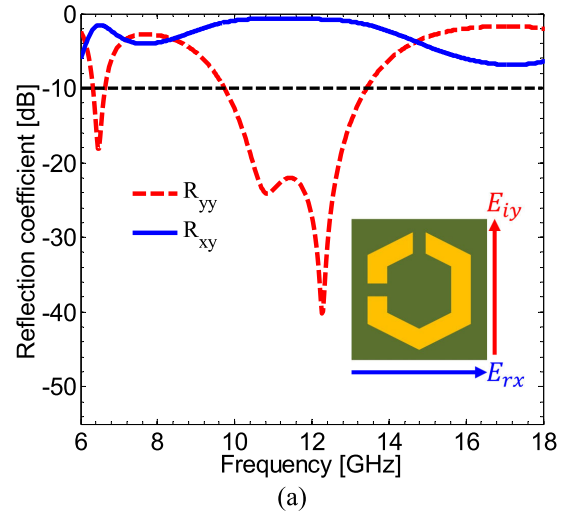where n is an odd integer. The linear-to-circular (LP-to-CP) polarization conversion is considered valid

even when the amplitude difference of the co- and cross-polarized components remains in the range of ± 3 dB $\left(-3\ \text{dB} \leq \left(|R_{xy}| - |R_{yy}|\right) \geq 3\ \text{dB}\right)$ while the phase difference satisfies

$$\Delta\emptyset = n^{\pi}/_2 \pm 10° \quad (2)$$

It can be seen from Fig. 3 that amplitude and phase difference criterion is perfectly fulfilled for LP-to-CP operation over three frequency bands 6.10-6.20, 6.84-9.02 and 14.10-15.48 GHz. The response of the metasurface for circularly polarized incident waves can be inferred from the reciprocity of the reflection coefficient matrix as $R^T = R$ where R^T is the transpose R. As the reflection coefficient matrix is reciprocal therefore metasurface maintains time-reversal symmetry and hence a circularly polarized incident wave is reflected as linearly polarized wave in the frequency bands 6.10-6.20, 6.84-9.02 and 14.10-15.48 GHz. The relation between linear and circular reflection coefficients, **R** an*d* **R**$_{cp}$ respectively,
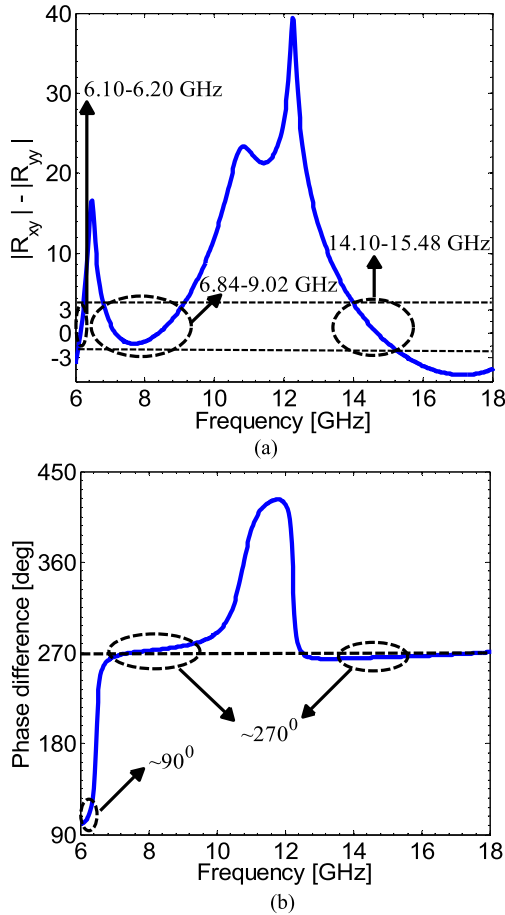
FIGURE 3. Difference between co- and cross-polarized reflection co-efficient (a) Magnitude (b) Phase.

is given by:

$$\mathbf{R_{CP}}$$
$$= \begin{pmatrix} R_{++} & R_{+-} \\ R_{-+} & R_{--} \end{pmatrix}$$
$$= \frac{1}{2} \begin{pmatrix} R_{xx} - R_{yy} - i\left(R_{xy} + R_{yx}\right) & R_{xx} + R_{yy} + i\left(R_{xy} - R_{yx}\right) \\ R_{xx} + R_{yy} - i\left(R_{xy} - R_{yx}\right) & R_{xx} - R_{yy} + i\left(R_{xy} + R_{yx}\right) \end{pmatrix}$$
(3)

where "+" stands for right-hand circular polarization (RHCP) and "−" for left-hand circular polarization (LHCP), R_{+-} represents reflection coefficient when incident wave is LHCP while reflected wave is RHCP.

By applying Stokes parameters, normalized ellipticity is determined to inquire the handedness of the reflected EMwave, as given in [50]. Normalized ellipticity ranges from +1 to −1. Whereas, ellipticity value of +1 indicates RHCP while −1 shows LHCP reflected wave. In Fig. 4 (a), it can be observed that the normalized ellipticity approaches +1, which shows that RHCP wave is reflected when the incident wave is linearly y-polarized.

Furthermore, above claim of RHCP is validated by polarization ellipses at multiple frequencies, where structure acts as a LP-to-CP converter. It can be elicited from Fig. 4 (bd)
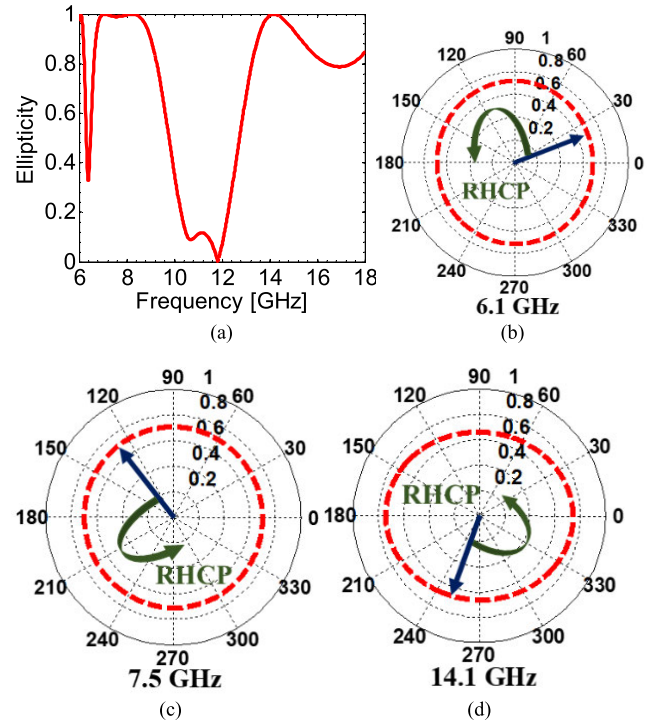

FIGURE 4. (a) Normalized ellipticity (b), (c) and (d) polarization ellipses at 6.1, 7.5 and 14.1 GHz.

that reflected wave is moving anti-clockwise, thus it is RHCP for all three bands of the operation 6.10-6.20, 6.84- 9.02, and 14.10-15.48 GHz.

C. ANGULAR STABILITY

The metasurface response is critically evaluated through its angular stability performance. Almost all applications require the response of the metasurfaces independent to the incidence angle of the impinging electromagnetic wave. We have analyzed and optimized our metasurface for different angles of incidence. Results for angular stability are shown in Fig. (5). The angularly stability for CPC operation has been demonstrated through polarization conversion ratio (PCR) which is defined as:

$$PCR = \frac{|R_{xy}|^2}{|R_{xy}|^2 + |R_{yy}|^2} \quad (4)$$

It can be seen form Fig. 5 (a) that PCR exceeds 90% over frequency bands 10.54-13.56 and 6.36-6.59 GHz at normal incidence, and at oblique angles, PCR ensures approximately the same response up to 45°. Similarly, Fig 5 (b)-(c) shows that within all three bands (6.10-6.20 GHz, 6.84-9.02 GHz and 14.10-15.48 GHz), the criterion of LP-to-CP conversion is satisfied for both magnitude and phase. Thus, the proposed design achieves a good angular stability for linear and circular polarization transformations.

IV. THEORETICAL ANALYSIS

To understand the operating principle of polarization conversion, we need to find out eigen-polarizations and eigenvalues
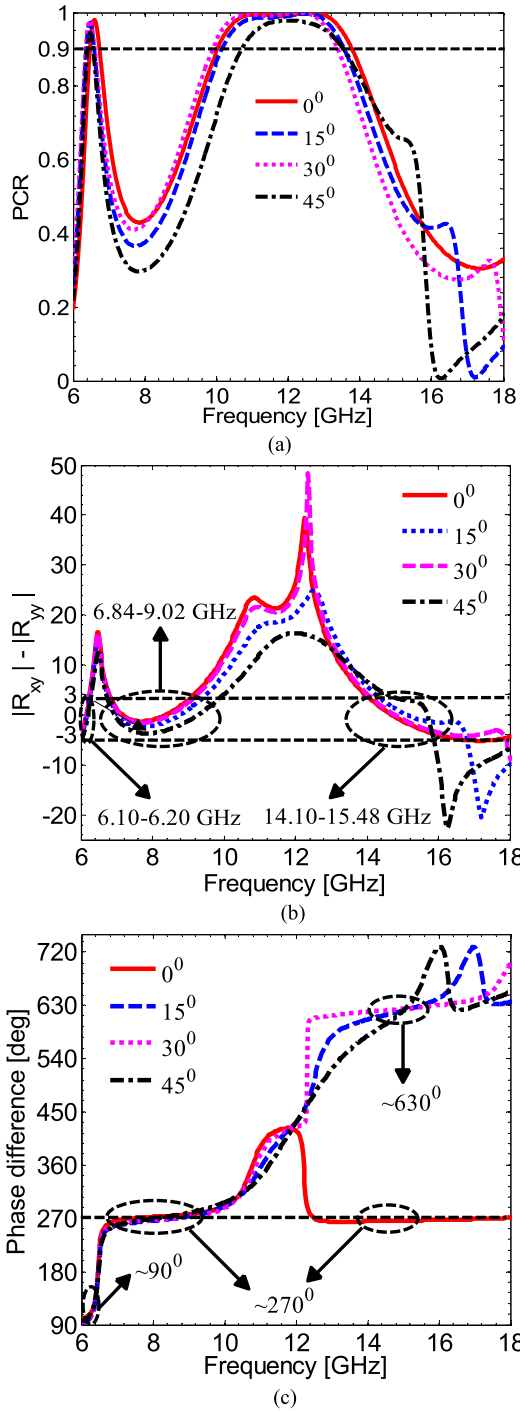
FIGURE 5. Difference between co- and cross-components of reflected wave at oblique angles (a) Magnitude (b) Phase (c) Polarization conversion ratio (PCR) for oblique angles.

FIGURE 6. (a) Decomposition of *y*-axis into *u*- and *v*-component (b) Magnitude plot of co-polarized reflection coefficients R_{uu} and R_{vv} (c) Phase difference between *u* and *v* reflected waves.

for our proposed design. To do this, we need to solve,

$$RX - mX = 0 \qquad (5)$$

where R is the reflection coefficient matrix, X is the eigenvector while m is the eigenvalue. Eq. 5 is solved at three resonance frequencies of 6.6 GHz, 11 GHz and 12.5 GHz where co-polarized reflection coefficient is negligible.
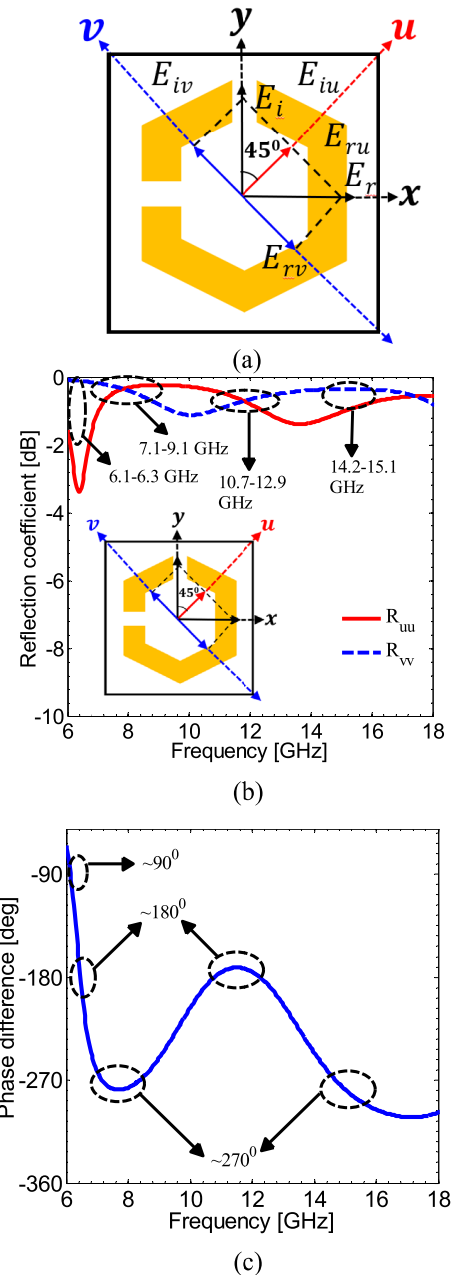
The obtained linearly independent eigenvectors are $X_1 = u = (1 \quad 1)^T$ $X_2 = v = (-1 \quad 1)^T$ with eigenvalues $m_1 = e^{i0} = 1$ and $m_2 = e^{i\pi} = -1$ respectively. Physically, this implies that the incident linearly polarized wave along u and v axis, which are oriented at $\pm 45°$ to the *y*-axis, shown in Fig. 6(a), is reflected without any polarization conversion. Moreover, the wave along u-axis is reflected with no phase change while the one along v-axis is reflected with 180° phase difference (along–v axis). Hence, the surface behaves as a high impedance surface (HIS), for one eigen-polarization while as a perfect electric conductor (PEC) for the other
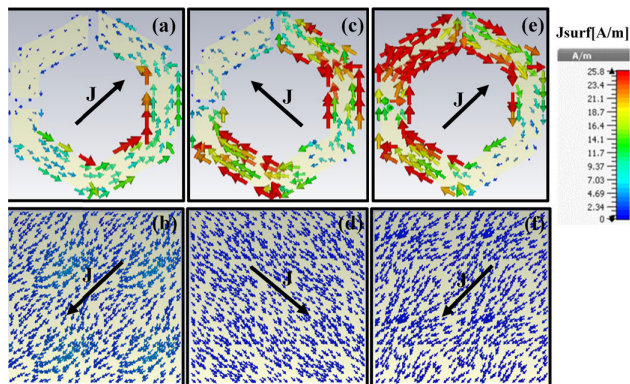
FIGURE 7. Surface current distributions on top layer and metallic ground plane at three different resonant frequencies: (a)-(b) 6.4 GHz (c)-(d) 10 GHz (e)-(f) 13.5 GHz.

FIGURE 8. Parametric study versus split width '*d*', the difference between reflection coefficient magnitudes.

FIGURE 9. Parametric study versus arm width '*w*', the difference between reflection coefficient magnitudes.

orthogonal eigen-polarization. As shown in Fig.6 (b)-(c), when the *u*- and *v*- components, E_{iu} and E_{iv}, of a *y*-polarized incident field, $E_i = \hat{y}E_i e^{i(kz+\omega t)}$ at $z = 0$ (metasurface plane) are reflected with zero phase (along *u*-axis) and 180° out of phase (along −*v*-axis), then the vector sum of the reflected field is along *x*-axis and hence the y-polarized wave becomes $x-$ polarized.

To verify the above theoretical analysis, numerical simulations were carried out for *u*- and *v*-polarized incident waves and the results are shown in Fig. 6 (b)-(c). It can be seen that the magnitude of the co-polarized reflection coefficients R_{uu} and R_{vv} is almost unity while the phase difference between the reflected *u*- and *v*- polarized field is 180° in accordance with our theoretical analysis for CPC operation. Moreover, in the frequency bands 6.10-6.20 GHz, 6.84-9.02 GHz and 14.10-15.48 GHz, $|R_{uu}| \approx |R_{vv}|$ while the phase difference is odd multiple of 90° leading to LP-to-CP conversion for *x*- or *y*-polarized incidence.

To elaborate further on the physical mechanism behind the polarization transformation, we study the surface currents on the metasurface at resonance frequencies. The impinging electromagnetic wave induces surface currents on the metasurface, which are coupled due to the bi-anisotropy of the unit cell through:

$$\begin{bmatrix} J \\ M \end{bmatrix} = i\omega \begin{bmatrix} \alpha_{ee} & \alpha_{em} \\ \alpha_{me} & \alpha_{mm} \end{bmatrix} \begin{bmatrix} E \\ H \end{bmatrix} \quad (6)$$

where, $J = [J_x, J_y]^T$ and $M = [M_x, M_y]^T$ are the electric and magnetic surface current densities respectively and ω is the angular frequency, $\alpha_{e,m}$ are electric and magnetic polarizability. We have assumed time variation of the form $e^{i\omega t}$ here. The electric and magnetic response gives the metasurface effective impedance given by (7)

$$Z(\omega) = \sqrt{\frac{\mu(\omega)}{\varepsilon(\omega)}} \quad (7)$$

where, $Z(\omega)$ is the surface impedance of the metasurface, and $\mu(\omega)$ and $\varepsilon(\omega)$ are magnetic permeability and electric permittivity respectively, all the three parameters are depending on
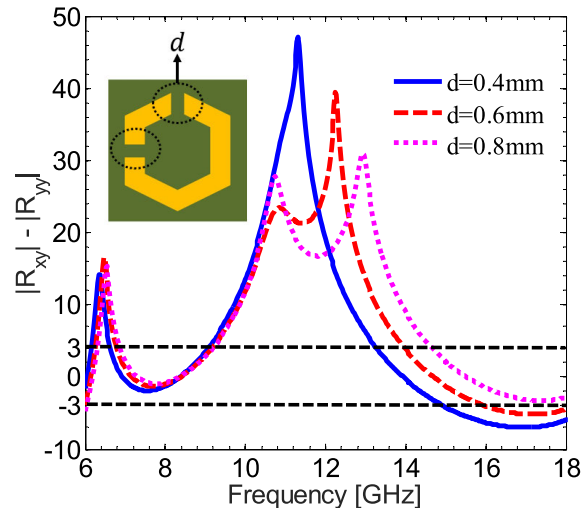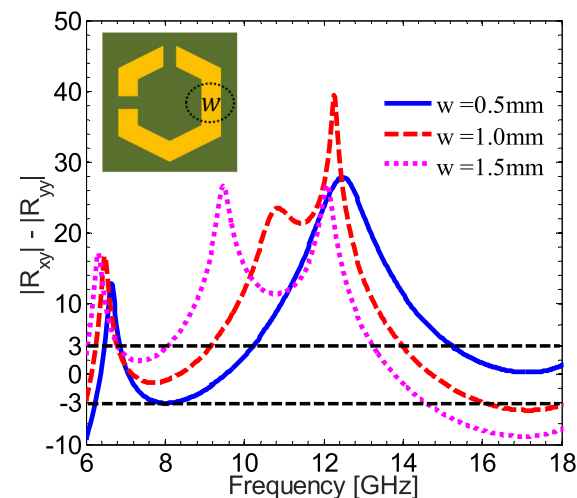
frequency. The reflection coefficient at normal incidence is given by:

$$R(\omega) = \frac{Z(\omega) - Z_o}{Z(\omega) + Z_o} \quad (8)$$

where $R(\omega)$ is complex reflection coefficient having both real and imaginary parts, Z_o is the impedance of free space and is 377Ω. Fig. 7 shows the surface current distribution at the top and bottom layer of the metasurface at resonance frequencies 6.4, 10 and 13.5 GHz for *u*- and *v*-polarizations.

It can be seen from Fig. 7, that at all three resonances, the currents at the top and bottom layer are anti-parallel which gives rise to a strong magnetic field inside the substrate sandwiched between the two layers. Due to strong magnetic field, the effective magnetic permeability gets large value and hence the effective impedance of the metasurface becomes much larger than free space impedance, $Z(\omega_r) \gg Z_o$
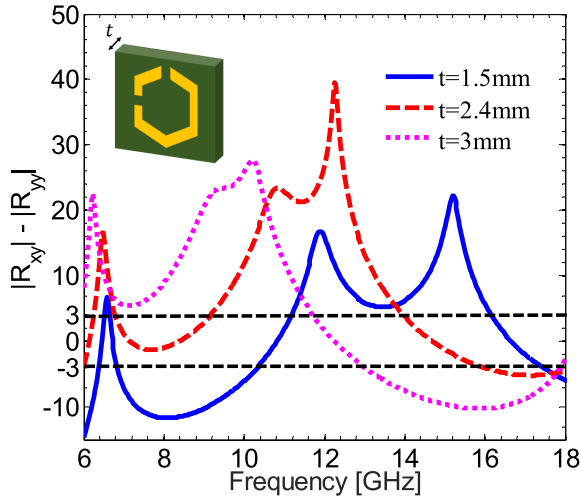
FIGURE 10. Parametric study versus substrate thickness '*t*', the difference between reflection coefficient magnitudes.

where ω_r the resonance frequency is. Under this condition, the reflection coefficient is near to unity, $R(\omega_r) \approx 1$ and hence the surface behaves as a high impedance surface (HIS) or artificial magnetic conductor (AMC) which is required for cross-polarization transformation.

V. PARAMETRIC ANALYSIS
In this Section, the metasurface response against some critical unit cell dimensions is analyzed. These dimensions include split width, arm width and substrate thickness. The numerical results shown in Fig. 8-10 are obtained to vary these three dimensions around their optimized values.

The effect of split width by varying its dimension from optimized value i.e. $d = 0.6$ mm is shown in Fig. 8. It should be noted that for a smaller value of $d = 0.4$mm, the capacitance between the gap increases thus shifting the response towards lower frequencies. For $d = 0.8$mm the metasurface has less capacitance and hence the resonant frequency shifts towards higher frequencies.

Another critical parameter of the proposed metasurface is the width of hexagonal arm. The difference between the magnitudes of reflections coefficients can be analyzed from Fig. 9 as the width of arm is changed from 0.5 mm to 1.5 mm. For $w = 0.5$ mm, the inductance of the patch gets lower resulting in a shift of resonant frequency to the higher values. Similarly, at larger dimension of w i.e. 1.5 mm, the arm inductance is increased thus resonating the unit cell at lower frequency band.

The thickness of the dielectric substrate is also an important parameter. In order to achieve both CPC and LP-CP operations, the substrate thickness is optimized at $t = 2.4$ mm. According to Maxwell's scale invariance, there is an inverse relation between the substrate thickness and resonant frequency. The thickness of the substrate has to be minimum for the unit cell to be resonating at higher frequencies. As shown in Fig. 10, if substrate thickness is increased to 3 mm, we get all resonances shifted towards lower frequencies.
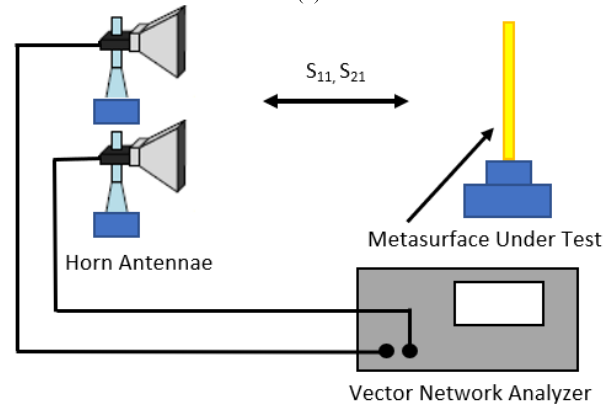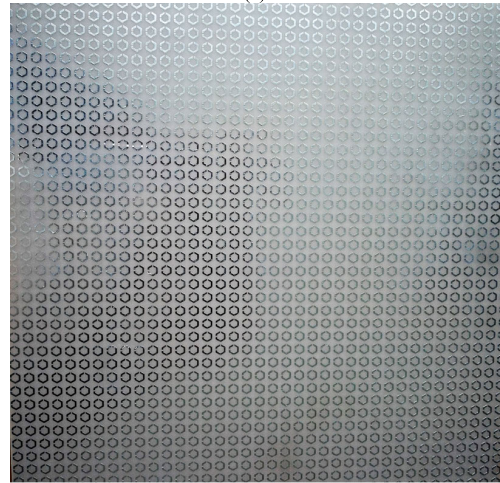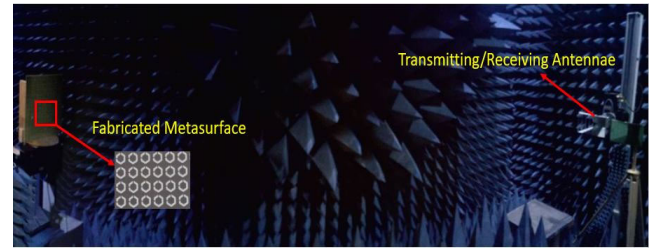

FIGURE 11. (a) Anechoic chamber experimental setup (b) Fabricated sample of metasurface (c) Schematic depiction of experimental setup.

If the substrate thickens is varied from the optimized value of 2.4 mm, the criterion of -3 dB magnitude difference of circular polarization is not achieved.

VI. MEASURED RESULTS
For experimental verification of the proposed design, metasurface was fabricated using PCB fabrication facility LPKF S103. The fabricated prototype is then tested in an in-house facility of fully anechoic chamber, as shown in Fig. 11 (a). The fabricated sample consists of 38×38 unit cells etched on the top of FR4 substrate having thickness of 2.4 mm, as shown in Fig. 11 (b). A schematic diagram of experimental setup is depicted in Fig. 11(c). Two double-ridge broadband horn antennas (OBH100400) and a vector network analyzer
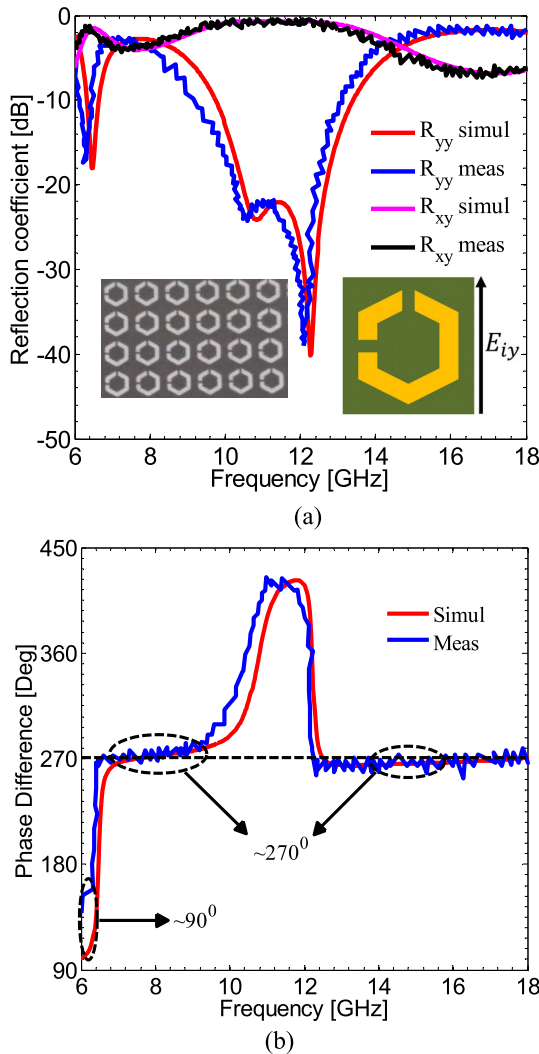
FIGURE 12. (a) Simulated and measured reflection coefficients when the incident field is *y*-polarized. Inset shows the fabricated metasurface. (b) Phase difference of co and cross-simulated and measured reflection coefficients when the incident field is *y*-polarized.

(HP 8722 C) were used for the measurement of reflection coefficients shown in Fig. 12 (a).

For measuring co-polarized coefficients, both transmitting and receiving horn antennas are placed along same orientation (vertical or horizontal) while for cross-polarization measurements they are placed orthogonal to each other. The measured results for the magnitude of co- and cross-polarized reflection coefficients and phase difference between the orthogonal components are presented in Fig. 12 (a) and (b) respectively. It can be seen from Fig. 12 that simulation results are consistent with the measurements. Small discrepancies in phase difference is due to the limitation of measurement setup and small size of the prototype.

VII. CONCLUSION
In this paper, a novel hexagonal multiband reflective metasurface showing CPC and LP-CP operations is presented.

The metasurface exhibits cross-polarization conversion (CPC) at two wide frequency bands from 6.36-6.59 GHz and 10.54-13.56 GHz. The CPC efficiency approaches 95% within these two operating bands. Moreover, linear-to-circular polarization conversion is achieved in three frequency bands: 6.10-6.20 GHz, 6.84-9.02 GHz and 14.10-15.48 GHz. The response of the designed metasurface is angular stable up to 45° of incidence angle. The compact size, angular stability and multiple functionalities make the proposed metasurface a potential candidate for many applications including miniaturized cavity resonators, chipless radio-frequency identification (RFID) tags, wave-guiding structures, RCS reduction, remote sensing and biomedical devices.

REFERENCES

[1] Y. Zheng, "Ultra-wideband polarization conversion metasurface and its application cases for antenna radiation enhancement and scattering suppression," *Sci. Rep.*, vol. 7, Nov. 2017, Art. no. 16137, doi: 10.1038/s41598-017-16105-x.

[2] H. Sun, "Broadband and broad-angle polarization-independent metasurface for radar cross section reduction," *Sci. Rep.*, vol. 7, Jan. 2017, Art. no. 40782, doi: 10.1038/srep40782.

[3] W. Chen, J. Gao, X. Cao, S. Li, and Z. Zhang, "A wideband multifunctional metasurface for antenna application," in *Proc. Asia–Pacific Conf. Antennas Propag. (APCAP)*, Jun. 2017, pp. 1–3.

[4] H. F. Ma, G. Z. Wang, G. S. Kong, and T. J. Cui, "Independent controls of differently-polarized reflected waves by anisotropic metasurfaces," *Sci. Rep.*, vol. 5, Apr. 2015, Art. no. 9605, doi: 10.1038/srep09605.

[5] M.-X. Ren, W. Wu, W. Cai, B. Pi, X.-Z. Zhang, and J.-J. Xu, "Reconfigurable metasurfaces that enable light polarization control by light," *Light, Sci. Appl.*, vol. 6, no. 6, pp. e16254–e16254, Jun. 2017, doi: 10.1038/lsa.2016.254.

[6] G. Singh, H. Sheokand, K. Chaudhary, K. V. Srivastava, J. Ramkumar, and S. A. Ramakrishna, "Fabrication of a non-wettable wearable textile-based metamaterial microwave absorber," *J. Phys. D, Appl. Phys.*, vol. 52, no. 38, Sep. 2019, Art. no. 385304.

[7] P. Munaga, S. Bhattacharyya, S. Ghosh, and K. V. Srivastava, "An ultra-thin compact polarization-independent Hexa-band metamaterial absorber," *Springer Appl. Phys. A*, vol. 124, p. 331, Apr. 2018.

[8] S. Ghosh and K. V. Srivastava, "Polarization-insensitive dual-band switchable absorber with independent switching," *IEEE Antennas Wireless Propag. Lett.*, vol. 16, pp. 1687–1690, 2017.

[9] M. Faenzi, G. Minatti, D. González-Ovejero, "Metasurface antennas: New models, applications and realizations," *Sci. Rep.*, vol. 9, Jul. 2019, Art. no. 10178.

[10] D. Samantaray, S. Bhattacharyya, and K. V. Srinivas, "A modified fractal-shaped slotted patch antenna with defected ground using metasurface for dual band applications," *Wiley Int. J. RF Microw. Comput.-Aided Eng.*, vol. 29, Dec. 2019, Art. no. e21932.

[11] Gao, X., "Bandwidth broadening of a linear polarization converter by near-field metasurface coupling," *Sci. Rep.*, vol. 7, Jul. 2017, Art. no. 6817, doi: 10.1038/s41598-017-07296-4.

[12] H.-Y. Chen, J.-F. Wang, H. Ma, S.-B. Qu, J.-Q. Zhang, Z. Xu, and A.-X. Zhang, "Broadband perfect polarization conversion metasurfaces," *Chin. Phys. B*, vol. 24, no. 1, Jan. 2015, Art. no. 014201.

[13] H. Dai, Y. Zhao, H. Sun, J. Chen, Y. Ge, and Z. Li, "An ultra-wideband linear polarization conversion metasurface," *Jpn. J. Appl. Phys.*, vol. 57, no. 9, Sep. 2018, Art. no. 090311.

[14] H. Chen, J. Wang, H. Ma, S. Qu, Z. Xu, A. Zhang, M. Yan, and Y. Li, "Ultra-wideband polarization conversion metasurfaces based on multiple plasmon resonances," *J. Appl. Phys.*, vol. 115, no. 15, Apr. 2014, Art. no. 154504, doi: 10.1063/1.4869917.

[15] V. S. Yadav, S. K. Ghosh, S. Bhattacharyya, and S. Das, "Graphene-based metasurface for a tunable broadband terahertz cross-polarization converter over a wide angle of incidence," *Appl. Opt.*, vol. 57, no. 29, p. 8720, Oct. 2018.

[16] S. Bhattacharyya, S. Ghosh, and K. V. Srivastava, "A wideband cross polarization conversion using metasurface," *Radio Sci.*, vol. 52, no. 11, pp. 1395–1404, Nov. 2017.

[17] M. Mutlu and E. Ozbay, "A transparent 90° polarization rotator by combining chirality and electromagnetic wave tunneling," *Appl. Phys. Lett.*, vol. 100, no. 5, Jan. 2012, Art. no. 051909.

[18] M. Feng, J. Wang, H. Ma, W. Mo, H. Ye, and S. Qu, "Broadband polarization rotator based on multi-order plasmon resonances and high impedance surfaces," *J. Appl. Phys.*, vol. 114, no. 7, Aug. 2013, Art. no. 074508.

[19] J.-L. Wu, B.-Q. Lin, and X.-Y. Da, "Ultra-wideband reflective polarization converter based on anisotropic metasurface," *Chin. Phys. B*, vol. 25, no. 8, Aug. 2016, Art. no. 088101.

[20] H. Sun, C. Gu, X. Chen, Z. Li, L. Liu, and F. Martín, "Ultra-wideband and broad-angle linear polarization conversion metasurface," *J. Appl. Phys.*, vol. 121, no. 17, May 2017, Art. no. 174902, doi: 10.1063/1.4982916.

[21] M. I. Khan, Q. Fraz, and F. A. Tahir, "Ultra-wideband cross polarization conversion metasurface insensitive to incidence angle," *J. Appl. Phys.*, vol. 121, no. 4, Jan. 2017, Art. no. 045103, doi: 10.1063/1.4974849.

[22] M. I. Khan and F. A. Tahir, "An angularly stable dual-broadband anisotropic cross polarization conversion metasurface," *J. Appl. Phys.*, vol. 122, no. 5, Aug. 2017, Art. no. 053103, doi: 10.1063/1.4997456.

[23] B. Lin, B. Wang, W. Meng, X. Da, W. Li, Y. Fang, and Z. Zhu, "Dual-band high-efficiency polarization converter using an anisotropic metasurface," *J. Appl. Phys.*, vol. 119, no. 18, May 2016, Art. no. 183103, doi: 10.1063/1.4948957.

[24] X. Gao, X. Han, W.-P. Cao, H. O. Li, H. F. Ma, and T. J. Cui, "Ultrawideband and high-efficiency linear polarization converter based on double V-shaped metasurface," *IEEE Trans. Antennas Propag.*, vol. 63, no. 8, pp. 3522–3530, Aug. 2015, doi: 10.1109/tap.2015.2434392.

[25] Y. Jia, Y. Liu, W. Zhang, and S. Gong, "Ultra-wideband and high-efficiency polarization rotator based on metasurface," *Appl. Phys. Lett.*, vol. 109, no. 5, Aug. 2016, Art. no. 051901, doi: 10.1063/1.4960355.

[26] J. Chen and A. Zhang, "A linear-to-circular polarizer using split ring resonators," *Appl. Comput. Electromagn. Soc. J.*, vol. 28, pp. 507–512, Jun. 2013.

[27] W. Cao, X. Yang, and J. Gao, "Broadband polarization conversion with anisotropic plasmonic metasurfaces," *Sci. Rep.*, vol. 7, Aug. 2017, Art. no. 8841, doi: 10.1038/s41598-017-09476-8.

[28] Z. Li, W. Liu, H. Cheng, S. Chen, and J. Tian, "Realizing broadband and invertible linear-to-circular polarization converter with ultrathin single-layer metasurface," *Sci. Rep.*, vol. 5, Dec. 2015, Art. no. 18106, doi: 10.1038/srep18106.

[29] B.-Q. Lin, J.-X. Guo, B.-G. Huang, L.-B. Fang, P. Chu, and X.-W. Liu, "Wideband linear-to-circular polarization conversion realized by a transmissive anisotropic metasurface," *Chin. Phys. B*, vol. 27, no. 5, May 2018, Art. no. 054204.

[30] M. T. Nouman, J. H. Hwang, and J.-H. Jang, "Ultrathin terahertz quarter-wave plate based on split ring resonator and wire grating hybrid metasurface," *Sci. Rep.*, vol. 6, Dec. 2016, Art. no. 39062, doi: 10.1038/srep39062.

[31] H. Zhao, "High-efficiency terahertz devices based on cross-polarization converter," *Sci. Rep.*, vol. 7, Dec. 2017, Art. no. 17882, doi: 10.1038/s41598-017-18013-6.

[32] H. L. Zhu, S. W. Cheung, K. L. Chung, and T. I. Yuk, "Linear-to-circular polarization conversion using metasurface," *IEEE Trans. Antennas Propag.*, vol. 61, no. 9, pp. 4615–4623, Sep. 2013.

[33] Y. Li, J. Zhang, S. Qu, J. Wang, L. Zheng, Y. Pang, Z. Xu, and A. Zhang, "Achieving wide-band linear-to-circular polarization conversion using ultra-thin bi-layered metasurfaces," *J. Appl. Phys.*, vol. 117, no. 4, Jan. 2015, Art. no. 044501.

[34] Li, Junhao, "Multiple-beam interference-enabled broadband metamaterial wave plates," *Phys. Rev. Appl.*, vol. 11, no. 4, 2019, Art. no. 044042.

[35] Chen, Lin, "Broadband wave plates made by plasmonic metamaterials," *Sci. Rep.*, vol. 8, no. 1, 2018, Art. no. 1051.

[36] C. Mao, Y. Yang, X. He, J. Zheng, and C. Zhou, "Broadband reflective multi-polarization converter based on single-layer double-L-shaped metasurface," *Appl. Phys. A, Solids Surf.*, vol. 123, p. 767, Dec. 2017, doi: 10.1007/s00339-017-1322-6.

[37] H. F. Ma, G. Z. Wang, G. S. Kong, and T. J. Cui, "Broadband circular and linear polarization conversions realized by thin birefringent reflective metasurfaces," *Opt. Mater. Express*, vol. 4, no. 8, pp. 1717–1724, 2014, doi: 10.1364/ome.4.001717.

[38] X. Huang, D. Yang, and H. Yang, "Multiple-band reflective polarization converter using U-shaped metamaterial," *J. Appl. Phys.*, vol. 115, Mar. 2014, Art. no. 103505, doi: 10.1063/1.4868076.

[39] X. Liu, "Three-band polarization converter based on reflective metasurface," *IEEE Antennas Wireless Propag. Lett.*, vol. 16, pp. 924–927, 2017, doi: 10.1109/lawp.2016.2614686.

[40] Z. Yin, F. Chen, L. Zhu, K. Guo, F. Shen, Q. Zhou, and Z. Guo, "High-efficiency dielectric metasurfaces for simultaneously engineering polarization and wavefront," *J. Mater. Chem. C*, vol. 6, no. 24, pp. 6354–6359, May 2018.

[41] L. Nama, S. Bhattacharyya, and P. K. Jain, "An ultra-thin wideband linear to circular polarization converter using metasurface," in *Proc. IEEE Int. Symp. Antennas Propag. USNC/URSI Nat. Radio Sci. Meeting*, Boston, MA, USA, Jul. 2018, pp. 777–778.

[42] W. Liu, "Highly efficient broadband wave plates using dispersion-engineered high-index-contrast subwavelength gratings," *Phys. Rev. Appl.* vol. 11, no. 6, 2019, Art. no. 064005.

[43] M. I. Khan, and A. T. Farooq, "A compact half and quarter-wave plate based on bi-layer anisotropic metasurface," *J. Phys. D, Appl. Phys.*, vol. 50, Oct. 2017, Art. no. 43LT04.

[44] Y. Zhuang, G. Wang, T. Cai, and Q. Zhang, "Design of bifunctional metasurface based on independent control of transmission and reflection," *Opt. Express*, vol. 26, pp. 3594–3603, Feb. 2018, doi: 10.1364/oe.26.003594.

[45] T. Cai, S.-W. Tang, G.-M. Wang, H.-X. Xu, Q. He, S. L. Sun, and L. Zhou, "Polarization-controlled bifunctional metasurfaces in transmission and reflection geometries," in *Proc. Prog. Electromagn. Res. Symp. (PIERS)*, Aug. 2016, pp. 2341–2342.

[46] J. Chen, "Integrating an ultra-broadband power splitter and a polarization converter using a zigzag metamaterial," *Opt. Mater. Express*, vol. 8, pp. 1454–1462, Jun. 2018, doi: 10.1364/ome.8.001454.

[47] J. H. Lee, "A semiconductor metasurface with multiple functionalities: A polarizing beam splitter with simultaneous focusing ability," *Appl. Phys. Lett.*, vol. 104, Jun. 2014, Art. no. 233505, doi: 10.1063/1.4883746.

[48] J. Zheng, "Highly anisotropic metasurface: A polarized beam splitter and hologram," *Sci. Rep.*, vol. 4, Sep. 2014, Art. no. 6491, doi: 10.1038/srep06491.

[49] M. I. Khan, and F. A. Tahir, "Simultaneous quarter-wave plate and half-mirror operation through a highly flexible single layer anisotropic metasurface," *Sci. Rep.*, vol. 7, Nov. 2017, Art. no. 16059, doi: 10.1038/s41598-017-15279-8.

[50] M. I. Khan, Z. Khalid, and F. A. Tahir, "Linear and circular-polarization conversion in X-band using anisotropic metasurface," *Sci. Rep.*, vol. 9, p. 4552, Mar. 2019, doi: 10.1038/s41598-019-40793-2.

MUHAMMAD SALMAN WAHIDI received the bachelor's degree in telecommunication engineering from MUET, Jamshoro, Pakistan, in 2016, and the M.S. degree in electrical engineering with majors in RF and microwave from NUST, Islamabad, Pakistan, in 2019. His research interests include metasurfaces and antennas.

M. ISMAIL KHAN received the bachelor's degree in computer systems engineering from the University of Engineering and Technology, Peshawar, in 2007, the M.S. degree in electronic engineering from the Capital University of Sciences and Technology, Islamabad, Pakistan, and the Ph.D. from the National University of Sciences and Technology, Pakistan. During the Ph.D. degree, his research was focused on design and analysis of metasurfaces for polarization control of GHz waves. He is working as an Assistant Professor with COMSATS University Islamabad, Pakistan. He is also working as a Postdoctoral Researcher with the School of Optics and Photonics, Beijing Institute of Technology, Beijing. His research interests include metasurfaces, metamaterials, antennas, quantum field theory, differential geometry, and complex manifolds.

FAROOQ A. TAHIR (Senior Member, IEEE) received the bachelor's degree in electrical engineering from the University of Engineering and Technology, Lahore, Pakistan, in 2005, the M.S. degree in RF telecommunications and microelectronics from the University of Nice, France, in 2008, and the Ph.D. degree from the National Research Center, University of Toulouse, France, in 2011. During the Ph.D. degree, his research was focused on electromagnetic modeling of large-size electronically reconfigurable reflectarrays. He has also been involved in the research project entitled R3MEMS funded by Thales Alenia Space. Under this project, he worked toward the development of RF MEMS-Based Microstrip Phase Shifter and its Equivalent Electrical Circuit. He is currently serving as an Associate Professor with the National University of Sciences and Technology, Islamabad, Pakistan. His research interests include reconfigurable, printed, and flexible antennas, metasurfaces, chipless RFID tags, and microwave medical devices. He is a Reviewer of many IEEE journals.

HATEM RMILI (Senior Member, IEEE) received the B.S. degree in general physics from the Science Faculty of Monastir, Tunisia, in 1995, the DEA Diploma degree in quantum mechanics from the Science Faculty of Tunis, Tunisia, in 1999, the Ph.D. degree in physics from the University of Tunis, Tunisia, and the Ph.D. degree in electronics from the University of Bordeaux 1, France, in 2004.

From December 2004 to March 2005, he was a Research Assistant with the PIOM Laboratory, University of Bordeaux 1. From March 2005 to March 2007, he was a Postdoctoral Fellow of the Rennes Institute of Electronics and Telecommunications, France. From March to September 2007, he was a Postdoctoral Fellow of the ESEO Engineering School, Angers, France. From September 2007 to August 2012, he was an Associate Professor with the Department of Electronics and Telecommunications, Mahdia Institute of Applied Science and Technology (ISSAT), Tunisia. He is currently a Full Professor with the Electrical and Computer Engineering Department, Faculty of Engineering, King Abdulaziz University, Jeddah, Saudi Arabia. His research interests concern applied electromagnetic applications involving antennas, metamaterials, and metasurfaces. His main targeted applications are reconfigurable antennas for multistandard wireless communications systems, security of chipless RFID systems with fractal tags, terahertz photoconductive antennas for infra-red energy harvesting, UWB nano rectennas for collection of solar energy, phase shifters for low-cost 5G communication systems, and microwave absorbing materials for stealth technologies.

● ● ●